Supplementary Information (SI) for Journal of Materials Chemistry C.

Supporting Information Section

Tailoring electromagnetic interference shielding, electrical and thermal properties of poly(vinylidene fluoride) based hybrid nanocomposites with carbon nanofiber and magnetite nanoparticles

Aleena Sabu[a,e], Sabarish Narayanan B[b], Pratheep Kumar Annamalai[c,d], Ramanujam Brahmadesam Thoopul Srinivasa Raghava[a,e,*]

a. *Department of Physics, Amrita School of Physical Sciences Coimbatore, Amrita Vishwa Vidyapeetham, India*
b. *Department of Electronics and Communication Engineering, Amrita School of Engineering, Amrita Vishwa Vidyapeetham, Coimbatore, India*
c. *Centre for Future Materials, University of Southern Queensland, Toowoomba QLD 4350, Australia*
d. *School of Agriculture and Environmental Science, University of Southern Queensland, Toowoomba QLD 4350, Australia*
e. *Functional Materials Laboratory, Amrita School of Engineering Coimbatore, Amrita Vishwa Vidyapeetham, India*

S1. Characterization

The X-ray diffraction (XRD) patterns of the synthesized magnetite nanoparticles, PVDF-CNF nanocomposites, PVDF-CNF-Fe_3O_4 hybrid nanocomposites and neat PVDF films with PVP are obtained through the XPERT-PRO model from Panalytical Instruments, UK. The analysis spanned a range of 2θ from 10° to 40°, where 'θ' represents the glancing angle. Since peaks corresponding to polymer are not found beyond 40^o, the XRD analysis has been carried out up to that angle for the nanocomposites. For neat PVP and magnetite nanoparticles, the 2θ range of 10^o to 80^o has been selected to show that PVP is indeed an amorphous material and peaks of magnetite nanoparticles are found beyond 70^o. To confirm the electroactive phase of PVDF and evaluate phase contents in the prepared nanocomposites, Fourier-transform infrared (FTIR) spectra of nanocomposites are recorded in attenuated total reflection (ATR) mode using the Alpha II model FTIR spectrometer from Bruker, USA. The resolution is better than 4 cm^{-1}, and the scan range is fixed between 450 cm^{-1} to 2000 cm^{-1} to confirm electroactive phases of PVDF. The FTIR scan range of synthesized magnetite nanoparticles is kept between 500 cm^{-1} to 4000 cm^{-1}. Crystallinity studies of solution blended PVDF-CNF and PVDF-CNF-Fe_3O_4 hybrid nanocomposites have been carried out through the differential scanning calorimeter (DSC)-Q20 model from TA Instruments, USA. The measurements are carried out under the nitrogen atmosphere, with heating and cooling rates set at 10 °C/min. The flow rate of nitrogen has been maintained at 50 ml/min. Thermal stability analysis of the prepared nanocomposites is carried out using the thermogravimetric analyser (TGA). The model is SDT Q600 TA Instruments, USA. The temperature is varied from room temperature to 900 °C at a ramp of 10 °C/min under nitrogen atmosphere, with a flow rate of 50 ml/min. The electrical resistances of the prepared nanocomposites are measured using a source meter (Model 2450 from Keithley, a Tektronics company, USA). A specially constructed brass holder has been used as the electrode for resistance measurements of the nanocomposites, and the thickness of the samples has been maintained at 0.1 mm. Impedance and dielectric studies on PVDF based nanocomposites are carried out using LCR meter model ZM2376 from NF Corporation, Japan. The UV-DRS spectrum corresponding to synthesized magnetite nanoparticles is obtained by using JASCO UV Vis (Model V-750) instrument in the wavelength range

800 – 200 nm. The magnetic properties of synthesized magnetite nanoparticles are measured at room temperature using Vibrating Sample Magnetometer (VSM) (model:7400 S series, Lake shore, UK). The saturation magnetization and coercivity can be deduced from the M-H curves obtained from VSM. The cross-section analysis of the representative PVDF-CNF and PVDF-CNF-Fe_3O_4 films are examined using a field emission scanning electron microscope (FE-SEM) (Gemini 300, Zeiss, Germany). Similarly, HRTEM analysis of selected PVDF-CNF and PVDF-CNF-Fe_3O_4 composites has been carried out using JEOL JEM 2100 with an operating voltage of 200 kV. The samples are ultramicrotomed using the instrument Leica EM FC7 to obtain a section thickness of 90 nm. Dynamic mechanical analysis measurement on neat PVDF, PVDF-9 wt% CNF and PVDF-9 wt% CNF-3 wt% Fe_3O_4 (all samples with 1 wt% PVP) has been conducted using TA Instruments Q800 system. The storage modulus (E') of the samples as a function of temperature has been measured in film tension mode, with a heating rate of 10 °C/min from 40 °C to 80 °C. For all samples, the amplitude of the dynamic stress and frequency were maintained at 0.1 MPa and 1 Hz, respectively. Scattering parameters at the X-band corresponding to PVDF-based binary and hybrid nanocomposites are measured using Anritsu spectrum analyser (Vector Network Analyser) from Tektronics company, USA, with a klystron-based X-band waveguide bench. From the measured scattering parameters, the electromagnetic interference shielding effectiveness of PVDF-based composites has been calculated and reported.

S2. Results and Discussion

S2.1. Dispersion of CNF and Fe_3O_4 nanoparticles in DMAc solvent and PVDF Matrix

To assess the dispersion of CNF and Fe_3O_4 within the PVDF matrix, a stability test has been conducted both with and without the addition of poly(vinylpyrrolidone) (PVP). Initially, 0.05 g each of CNF and Fe_3O_4 nanoparticles are probe-sonicated separately for 30 min in 8 ml of DMAc without surfactant. It is observed that CNF and Fe_3O_4 particles rapidly settled out, indicating poor dispersion in the chosen solvent namely DMAc. However, with the addition of 1 wt% of PVP, the dispersion remained stable for over 15 hours without agglomeration. This improved dispersion effect is further reflected in the solution blended PVDF-based nanocomposites namely PVDF-CNF, PVDF-Fe_3O_4, and PVDF-CNF-Fe_3O_4-with 1 wt% PVP (with respect to composite amount). In composites prepared without PVP, the CNF and Fe_3O_4 fillers are poorly dispersed in the polymer matrix, leading to noticeable agglomeration, consistent with the results of the stability test carried out in the solvent. In contrast, the addition of PVP resulted in uniform dispersion of the fillers, as evidenced by the formation of homogenous black films. Digital images of the prepared nanocomposites, including PVDF with 3 wt% CNF, PVDF with 3 wt% Fe_3O_4, and PVDF with 3 wt% CNF and 3 wt% Fe_3O_4, both with and without 1 wt% PVP, are shown in Fig. S1a–f. These images clearly demonstrate the fact that the presence of PVP significantly enhances the dispersion of CNF and Fe_3O_4 nanoparticles within the PVDF matrix, The enhanced dispersion of fillers in the polymer matrix is attributed to the interaction between the PVP chains and the nanofiller.

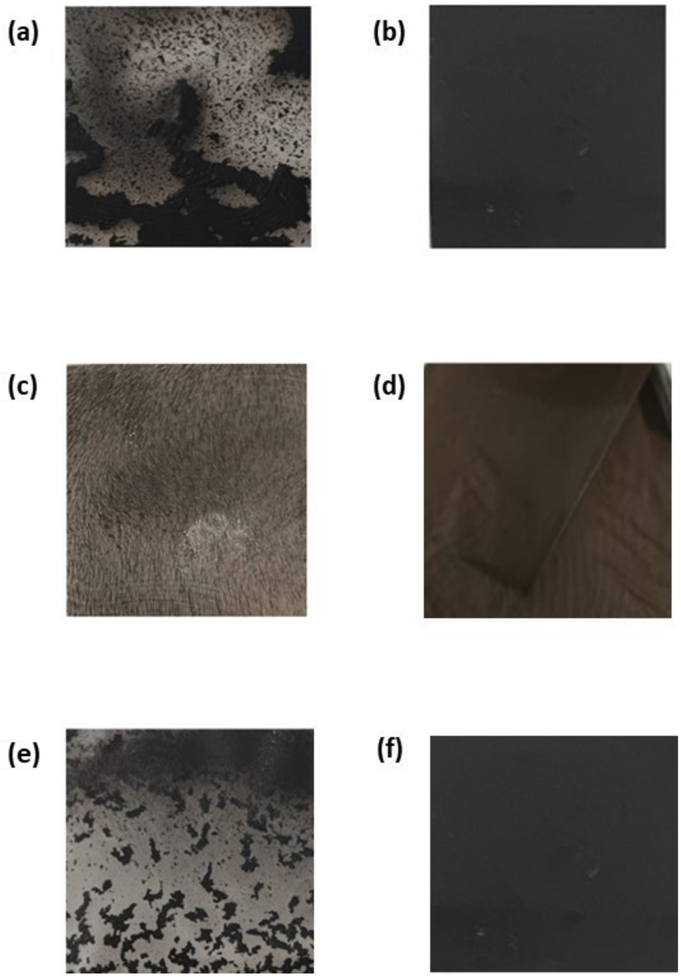

Fig. S1 Digital images of solution blended (a) PVDF-3 wt% CNF, (b) PVDF-3 wt% CNF-1 wt% PVP, (c) PVDF-3 wt% Fe_3O_4, (d) PVDF-3 wt% Fe_3O_4-1 wt% PVP, (e) PVDF-3 wt% CNF-3 wt% Fe_3O_4, and (f) PVDF-3 wt% CNF-3 wt% Fe_3O_4 -1 wt% PVP.

PVP has very good propensity towards carbon nanostructures as reported elsewhere[1] and hence improves the dispersion of carbon fillers in the selected solvent as well as in the polymer matrix. In a similar manner, PVP coated magnetite nanoparticles have been reported to be highly dispersible both in organic solvent and water.[2]

Fig. S2a and b illustrate the dispersion behaviour of CNF and Fe_3O_4 in DMAc solvent without PVP, where rapid settling of filler particles is evident after half an hour of probe sonication, whereas Fig. S2c and d show well-dispersed filler particles with the addition of PVP, and it is observed that the dispersion of the fillers is stable even after 15 hours as shown in Fig. S2e and f.

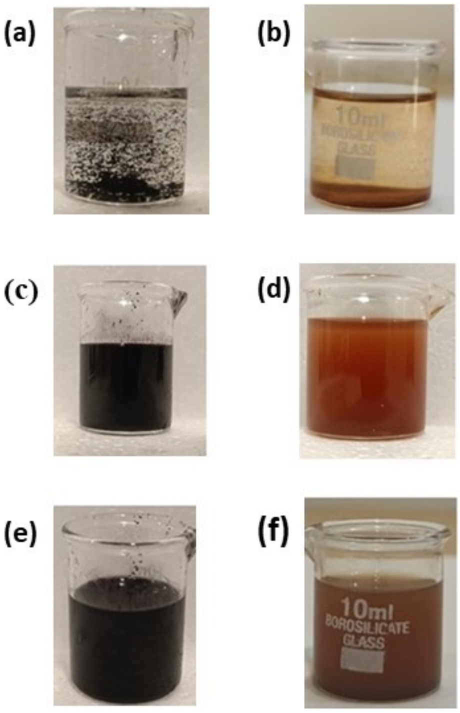

Fig. S2 Dispersion of (a) CNF, (b) magnetite nanoparticles in DMAc solvent without PVP, (c) CNF dispersion with PVP after 30 mins probe sonication, (d) magnetite dispersion with PVP after 30 mins probe sonication, (e) CNF dispersion with PVP after 15 hours probe sonication, and (f) magnetite dispersion with PVP after 15 hours probe sonication.

The quality of interfacial interaction between carbon nanofiber/magnetite nanoparticles with the polymer is dictated by the surface chemistry of CNF/magnetite and the matrix chosen. There are various methods reported in the literature for the dispersion of CNFs in different polymer matrices such as shear mixing, wrapping polymers, surface functionalization and employing surfactants[3]. Surface functionalization of filler is a destructive approach where functional groups are introduced onto the filler surface which can form the covalent bond with the chosen polymer matrix. The electronic conductivity of CNFs has been reported to be decreased after surface functionalization due to oxidation treatment[4] . Hence, surfactant (PVP) has been employed to improve the interfacial adhesion between the filler particles and the PVDF matrix and indeed we have proved that the dispersion of PVP capped CNF and magnetite nanoparticles is improved in the PVDF matrix as depicted in Fig. S1 and Fig. S2.

S2.2. AC conductivity, dielectric property and impedance analysis of solution blended PVDF-CNF nanocomposites

The AC conductivity of neat PVDF and PVDF-CNF (all samples with 1 wt% PVP) nanocomposite films have been investigated across the frequency range 10^3 to 10^6 Hz, as shown in Fig. S3a. The neat PVDF film with PVP exhibits typical frequency-dependent behaviour of an insulator as the conductivity increases with the frequency. It should be mentioned that the area of cross-section of films and the thickness are maintained the same for all compositions. It can be seen that when the loading of CNF is increased, a plateau region in frequency-dependent conductivity plot can be identified. The plateau region signifies DC conductivity and is essentially due to the network formation between CNFs. When the nanocomposite becomes more conducting, the interparticle distance between the filler particles would decrease, and hence, the real part of relative permittivity (ε') at lower frequencies shall be anticipated to be higher for highly conducting samples.

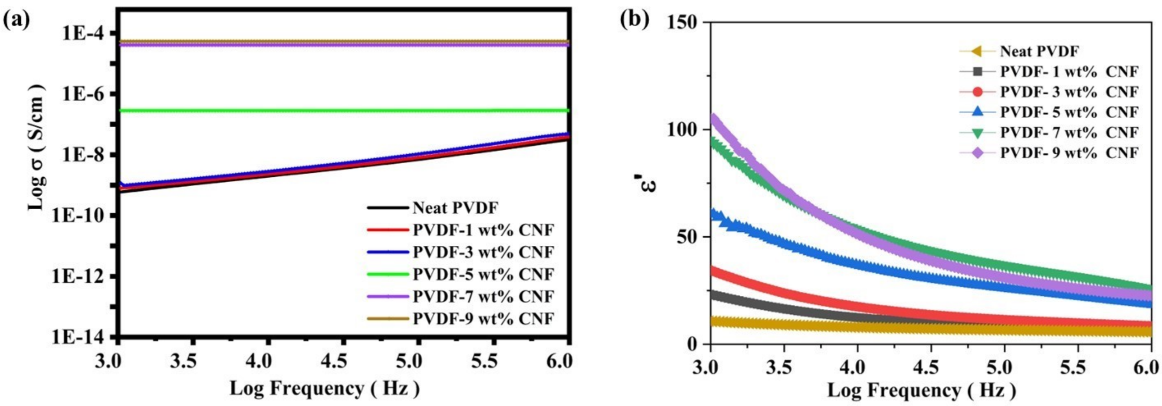

Fig. S3 (a) AC conductivity, and (b) real part of relative permittivity of PVDF-CNF nanocomposites.

The real part of relative permittivity is calculated using the following formula, $\sigma_{ac} = \varepsilon_{\circ}\, 2\pi f(\tan\delta)\varepsilon^{'}\#(S1)$

where $\varepsilon^{'}$ is the real part of relative permittivity, f is the frequency, σ_{ac} is the AC conductivity and $\varepsilon_{\circ}$ is the permittivity of free space[5]. Fig. S3b depicts the variation of $\varepsilon^{'}$ of PVDF-x wt% CNF-1 wt% PVP (x = 0,1,3,5,7,9) with respect to frequency. It can be seen from the plot that $\varepsilon^{'}$ decreases with increase in frequency. Also, $\varepsilon^{'}$ increases at 1 kHz up on adding CNF into the PVDF matrix. The increase in relative permittivity with CNF addition shall be attributed to Maxwell-Wagner-Sillars (MWS) polarization originating from the accumulation of space charges and/or dipoles at interfaces[6]. At lower frequencies, dipoles have sufficient time to align themselves under the direction of the electric field. However, at higher frequencies, the electric field changes too rapidly and the dipoles cannot respond immediately, resulting in a lower value of $\varepsilon^{'}$. Similar results have been reported for different polymer composite systems[7].

Since the $\varepsilon^{'}$ at lower frequencies increases with CNF addition, the interjection capacitance is anticipated to be higher for composites with higher loadings of CNF. To prove the above point, impedance measurements have been carried out on representative PVDF-CNF nanocomposites with 1 wt% PVP. Conducting polymer composites are modelled as parallel combination of resistor with resistance R_2 (bulk resistance) and capacitor with capacitance C_1 (interjection capacitance) with a series resistance R_1 accounting for the resistance between the fillers in contact. This model is validated by the occurrence of a semicircular response in the Argand plane when real and imaginary parts of impedances are plotted. It is also possible to get a depressed semicircle in the Argand plane because of surface roughness at the electrode-material interface [8]. The experimental data points in that case can be fitted by including a constant phase element (CPE) instead of a capacitor in the parallel model. In fact, the impedance behaviour of PVDF-CNF nanocomposites in the Argand plane results in a depressed semicircle as depicted in Fig. S4a-d. CPEs are employed to model the experimental data of impedance that deviates from ideal capacitive characteristics. The mathematical representation of CPE is given by [8].

$$Z_{CPE} = \frac{1}{\omega^n Q_o} \times e^{\frac{-\pi n i}{2}} \#(S2)$$

where 'Q_o' is the pre-exponential term, 'ω' is the angular frequency and 'n' is the exponent which varies between 0 and 1.

From the 'Q_o' and 'n' values, the capacitance can be calculated using the formula as reported elsewhere. [9]

$$C = R^{\frac{(1-n)}{n}} Q_0^{\frac{1}{n}} \#(S3)$$

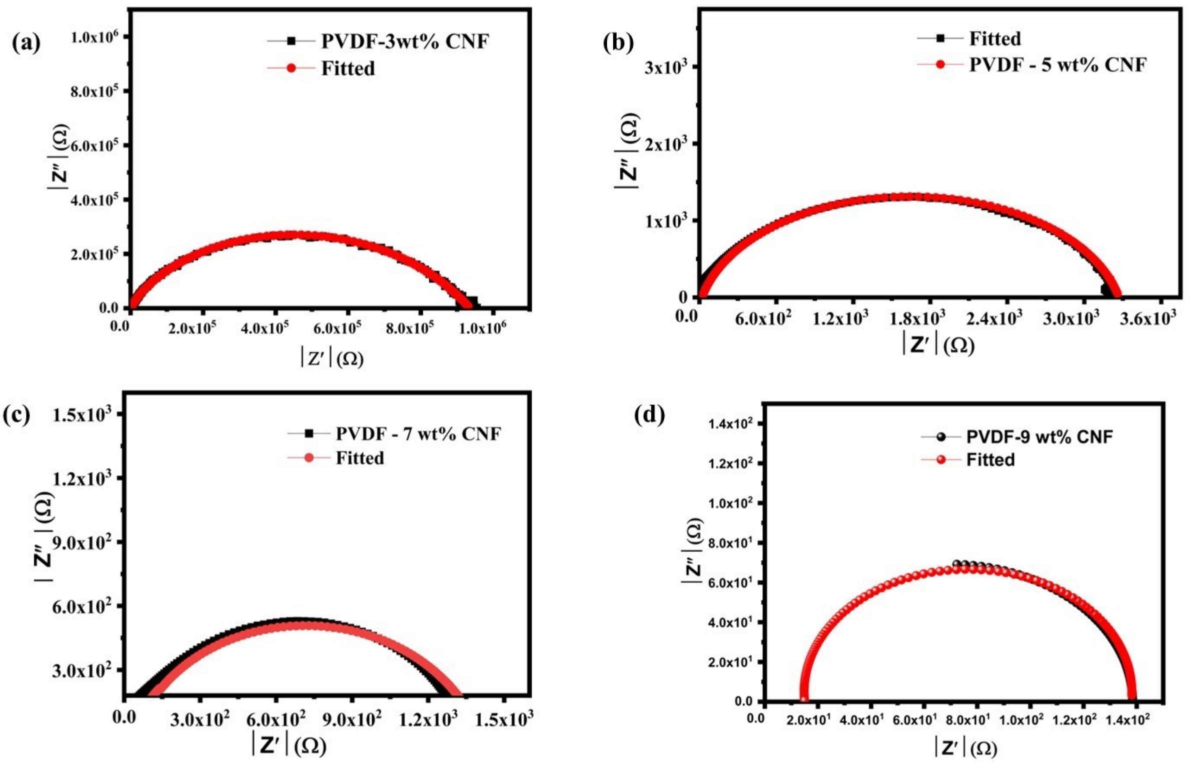

Fig. S4 (a)-(d) Impedance plots of solution blended PVDF-x wt% CNF (x=3,5,7,9) nanocomposite with 1 wt% PVP.

Impedance response of PVDF-3 wt% CNF, PVDF-5 wt% CNF, PVDF-7 wt% CNF, and PVDF-9 wt% CNF with 1 wt% PVP are shown in Fig. S4a- d respectively. The experimental data points of impedance when plotted in the Argand plane corresponding to different frequencies are fit using EIS analyser software, with fit parameters presented in Table S1. The equivalent circuit as shown in Fig. S4e has been used to fit the experimental data points.

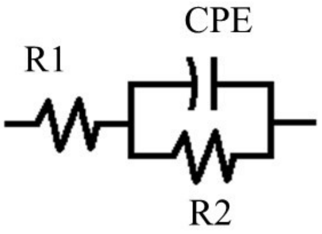

Fig. S4 (e) Schematic of the proposed equivalent circuit.

The depressed semicircular behaviour observed for all materials has been taken care of by including CPE in the equivalent circuit. The actual capacitance value, calculated from parameters such as 'Q_o' and 'n' values reveal the fact that the interjection capacitance of PVDF based nanocomposites has been increased with CNF loading in PVDF, supporting the real part of the relative permittivity analysis of PVDF-CNF composites. For the insulating PVDF-3 wt% CNF composite with PVP, the interfacial capacitance calculated is 5.43 x 10^{-3} pF. With increasing loading of CNF, the interfacial capacitance increases which is primarily attributed to a greater number of interfaces formed where the charges can be accumulated. For PVDF-9 wt% CNF-1 wt% PVP, the interfacial capacitance obtained is 7830 pF which is far higher than that obtained for 3 wt% CNF loading in PVDF. Further, the interparticle distance between filler particles decreases when CNF loading in the polymer matrix is increased which eases the charge transport resulting in the enhancement of electrical conductivity. Also, it is worth noting that the bulk resistance (R_2) and the contact resistance between filler particles (R_1) of the composite decrease with an increase in CNF loading essentially due to the network formation between filler particles. It should be mentioned here that the thickness of the PVDF-CNF films with PVP is maintained at 0.1 mm.

Table S1 Parameters extracted from impedance plots of PVDF-x wt% CNF (x=3,5,7,9) with 1 wt% PVP after fitting to parallel model.

Sample	**Q_0 (S^n Ω^{-1})**	**R_1 (Ω)**	**R_2 (Ω)**	**n**	**C (pF)**
PVDF-3 wt% CNF	7.96×10^{-11}	5011	9.18×10^{5}	0.654	0.00543
PVDF-5 wt% CNF	2.54×10^{-10}	70	3220	0.864	14.9
PVDF-7 wt% CNF	7.45×10^{-9}	52	1354	0.772	99.6
PVDF-9 wt% CNF	9.19×10^{-8}	15	123	0.99	7830

S2.3. FTIR analysis of solution-blended PVDF-CNF nanocomposites

The quantification of the electroactive phase in PVDF-CNF nanocomposites with PVP and neat PVDF with and without PVP has been carried out using the formula given below in equation eqn (S4) as reported elsewhere[10],

$$F(\gamma) = \frac{A_\alpha}{\left(\frac{k_\gamma}{k_\alpha}\right) A_\alpha + A_\gamma} \#(S4)$$

where k_γ and k_α are the absorption coefficients, while A_γ and A_α are the absorbances at 833 cm^{-1} and 763 cm^{-1} respectively [10] . The FTIR spectra of PVDF-CNF nanocomposites with 1 wt% PVP have been presented in the main manuscript under section 3.2. The compositional dependence of the electroactive gamma phase content is tabulated in Table S2. It should be mentioned that the FTIR spectrum for each composition is obtained from three different regions of the same film and the electroactive phase content is calculated along with the error. The result obtained from FTIR for gamma fraction in the composites is also validated through the ratio of area under the melting curves (gamma to alpha phase) (A_γ/A_α) as discussed in the DSC analysis section.

Table S2 Quantification of electroactive gamma phase content in solution blended neat PVDF, PVDF-x wt% CNF-1 wt% PVP (x=0,1,3,5,7,9) films.

Sample	**Gamma phase fraction (%)**
Neat PVDF	70.8 ± 1.0
PVDF-1 wt% PVP	94 .0± 1.4
PVDF-1 wt% CNF-1 wt% PVP	74.2 ± 1.8
PVDF-3 wt% CNF-1 wt% PVP	91.5 ± 0.6
PVDF-5 wt% CNF-1 wt% PVP	88.7 ± 1.1
PVDF-7 wt% CNF-1 wt% PVP	83.2 ± 0.4
PVDF-9 wt% CNF-1 wt% PVP	84.3 ± 0.2

The gamma phase content in neat PVDF film is ~70.8%. For PVDF-1 wt% PVP, the electroactive gamma phase content is increased to 94%. The result suggests that PVP has better interaction with PVDF. The carbonyl group of PVP and CH_2 group of PVDF [11] can interact well which results in gamma phase conformation leading to higher gamma phase content.

When 1 wt% CNF is incorporated in PVDF with PVP, and the electroactive gamma phase content is decreased to 74.2%. This can be attributed to the interaction between CNF and PVP which is greater than the interaction between PVDF and PVP. Hence PVP chains can coil around CNF completely and the PVP coated CNF would be distributed in the PVDF matrix. Since neither CNF nor PVP has direct interaction with PVDF, the electroactive phase content is decreased to 74.2%. This is slightly higher than that of neat PVDF. This situation is depicted in the model proposed as shown in Fig. S5c. In Fig. S5a and S5b, neat PVDF chains and PVDF-PVP chains are depicted. Since at lower loading of CNF, the number of CNF particles would be lesser, not all the PVP chains would have been used for coating the filler and hence some of them will still be with PVDF matrix which results in gamma phase content to be higher than that of neat PVDF film due to the interaction between PVP and PVDF. At 3 wt% CNF loading in PVDF, the electroactive gamma phase is enhanced to 91.5% in comparison to neat PVDF film. It should be mentioned that 3 wt% CNF loading is just nearer to the percolation threshold, and the alignment of PVP-coated CNF begins, which requires a lesser number of PVP molecules to coat many CNFs. This situation makes more PVP molecules to interact with PVDF chains resulting in enhanced electroactive gamma phase content $F(\gamma)$. This scenario is depicted in Fig. S5d. However, the value of $F(\gamma)$ is less than that of PVDF-1 wt% PVP composite film. At 5 wt% CNF loading in PVDF with PVP, the $F(\gamma)$ is reduced considerably to 88.7% which is lesser than that of PVDF-1 wt% PVP and 3 wt% CNF loading in PVDF with PVP. Since 5 wt% CNF loading in PVDF is above the percolation threshold, more networks would have formed and hence more number of PVP chains will be required to coil the filler particles in comparison to 3 wt% CNF loading in PVDF. Thus, the $F(\gamma)$ is reduced. This situation is depicted in Fig. S5e. However, the phase content is higher than that of neat PVDF film without PVP. With increasing CNF loading to 7 wt%, the $F(\gamma)$ is reduced in comparison to 3 wt%, 5 wt% CNF loaded PVDF samples with PVP which signifies more and more

PVP chains would have coiled the CNF particles and a smaller number of PVP would still remain with the matrix as depicted in Fig. S5f. Hence, F(γ) is reduced. However, the value is higher than that of neat PVDF film. In the case of PVDF-9 wt% CNF-1 wt% PVP, F(γ) slightly increases to 84.3% in comparison to 7 wt% CNF loading in PVDF. As the number of network formation between the fillers and the number of filler particles is increased in the PVDF matrix, the F(γ) would have been anticipated to be lesser than other compositions. This result shows that for 9 wt% CNF incorporation in PVDF results in a greater number of PVP molecules to coat the filler particles and there can be a possibility of incomplete coating of CNF by PVP molecules as depicted in Fig. S5g. The CNF particle's edges could be interacting with PVDF chains. Since π electrons of CNF can interact well with PVDF chains causing a slight increase in F(γ) i.e., 84.3% . This value is higher than that of neat PVDF. Though in PVDF-9 wt% CNF composite with PVP, a greater number of CNF particles could be randomly distributed in the PVDF matrix, the interaction between CNF and the matrix makes F(γ) to be higher than that of neat PVDF. If PVP coats CNF particles well, the interaction between CNF with PVDF will be screened and hence, CNF cannot act as a nucleating agent. If this proposed mechanism is true then, the crystallization temperature should be decreased when CNF is incorporated in PVDF along with PVP. This is indeed observed in the DSC analysis. However, there is a small increase in crystallization temperature for 9 wt% CNF loading in PVDF that is why at this loading it has been highlighted that the interaction of PVDF chains with filler edges would be significant. The entire sequence is clearly depicted by a model as shown in Fig. S5.

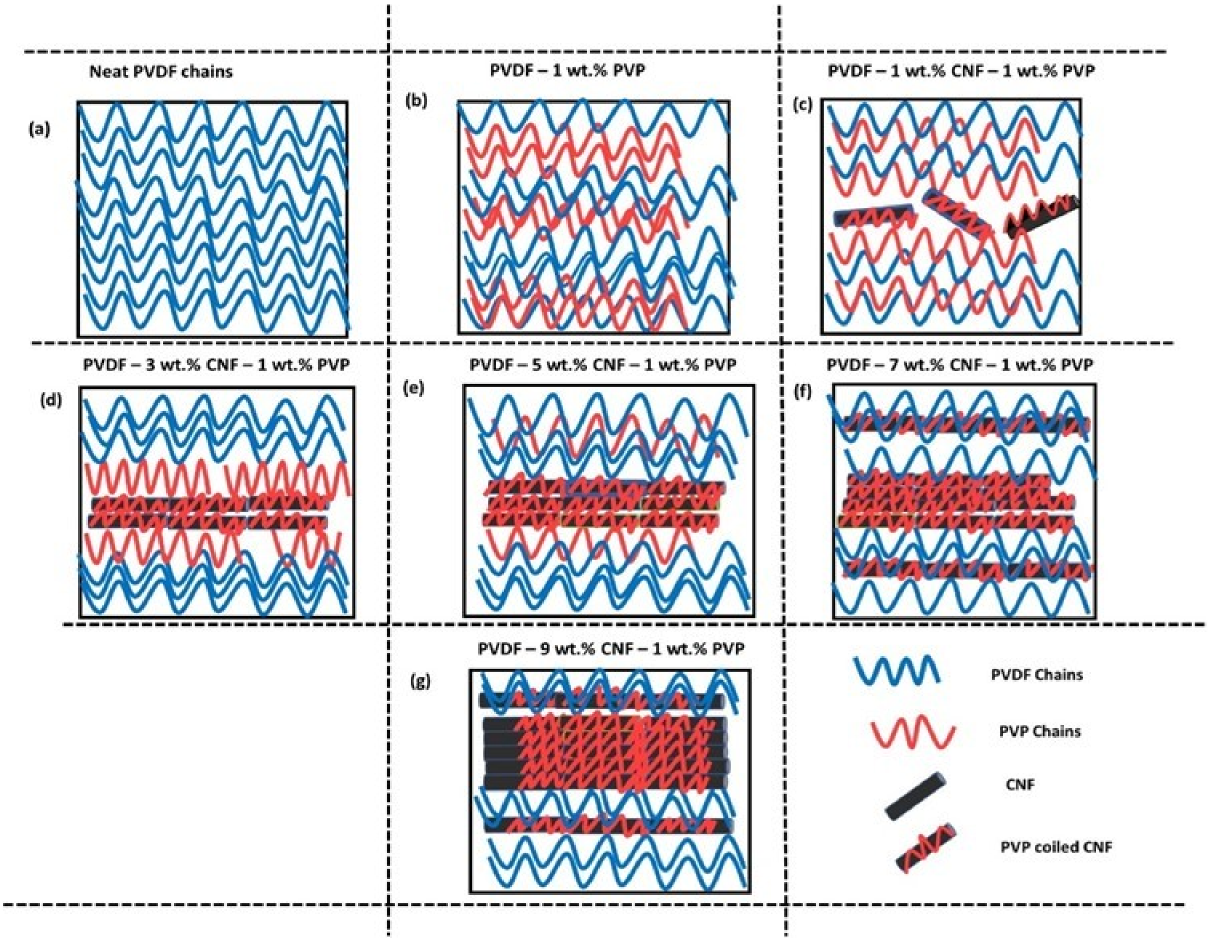

Fig. S5 Model depicting the interaction between PVDF, CNF and PVP.

S2.4. DSC analysis of solution-blended PVDF-CNF nanocomposites

In order to confirm the coexistence of electroactive gamma and non-polar alpha phases of PVDF in PVDF-CNF-PVP nanocomposites, DSC analysis of PVDF-x wt% CNF (x = 0,1,3,5,7,9) with 1 wt% PVP and neat PVDF without PVP has been carried out. Fig. S6a and b depict the crystallisation and melting curves while Fig. S7 depicts the endothermic melting curves of the above-mentioned composites. The melting curves have been deconvoluted into two peaks using the Gaussian function for various nanocomposites. The low-temperature melting peak (~162 °C) corresponds to the non-polar alpha phase and the high-temperature melting peak (~170 °C) corresponds to the electroactive gamma phase as reported elsewhere [10]. It can also be seen that the area under the gamma phase melting curve is higher in comparison to alpha phase melting curve supporting the FTIR result. Table S3 details the area under the alpha and gamma phase melting curves of PVDF after deconvoluting the respective melting curves. The ratio of area under gamma (A_γ) to alpha (A_α) phase melting curves follows a similar trend as that of electroactive phase content obtained through FTIR analysis which is shown in Fig. S8. Thus, the DSC results are corroborating with XRD and FTIR results.

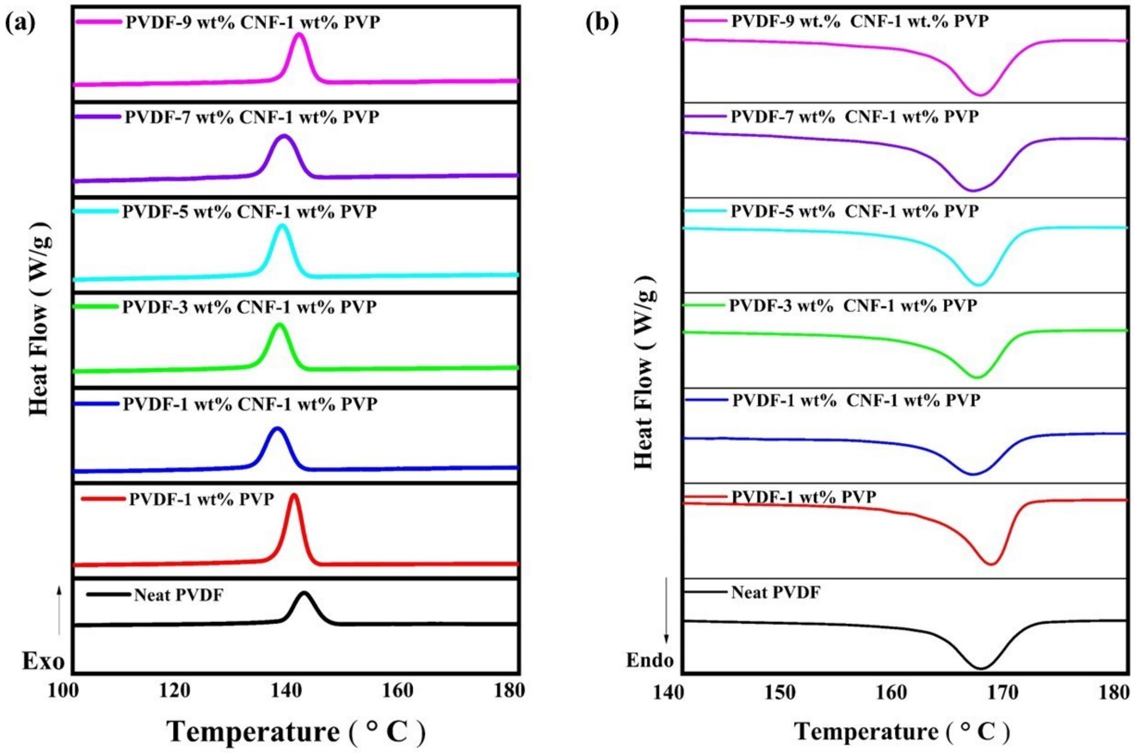

Fig. S6 (a) Crystallization, and (b) melting curves of PVDF-CNF solution blended nanocomposites with PVP.

Table S3 describes the degree of crystallinity, crystallization temperature and the ratio of area under the gamma phase melting curve to alpha phase melting curve of PVDF in nanocomposites after deconvoluting the melting curves of various PVDF-CNF-PVP nanocomposites. The degree of crystallinity is calculated using the relation reported elsewhere. [12] The enthalpy of crystallization corresponding to 100% crystallized PVDF is taken to be 104.5 J/g . [13] The crystallinity of neat solution blended PVDF film is 43.64% without PVP. With PVP incorporation, the percentage crystallinity is slightly decreased along with T_c in comparison to that of neat PVDF. It seems that the molecular weight of PVDF, PVP and the conditions employed in the preparation method can affect the crystallinity. Drastic reduction in the percentage of crystallinity is observed for PVDF-1 wt% CNF nanocomposites in comparison to neat PVDF. As a matter of fact, the crystallinity is decreased when CNF is incorporated in PVDF. In view of the FTIR analysis, the DSC data also follows a similar trend. Since the number of CNF particles will be lesser at 1 wt% loading, the PVP molecules can completely coat the filler, and the PVP-coated CNF would have been dispersed in such as fashion that they occupy interchain PVDF space. Hence the crystallinity is reduced drastically. When CNF loading is 3 wt% which is the loading just nearer the percolation threshold, the random distribution of PVP coated CNF will be reduced. On evaporating the solvent, the PVDF chains can come closer and hence the crystallinity is increased (30.14 %) in comparison to 1 wt% CNF loading. However, the value is lesser than that of neat PVDF film with and without PVP. For PVDF-5 wt% CNF-1 wt% PVP, the percentage of crystallinity further decreases to 25.58% which is attributed to the fact that more number of network formation would have resulted due to an increase in CNF loading. The number of PVP-coated CNF occupying inter-PVDF chains would be lesser in comparison to 1 wt% CNF loading which is why the percentage of crystallinity is increased in comparison to 1 wt% CNF loaded PVDF. However, in comparison to 3 wt% CNF loading in PVDF, the crystallinity is decreased for 5 wt% CNF loaded PVDF. For PVDF-7 wt% CNF with PVP, the number of CNF particles coated with PVP not used for network formation can occupy random positions in between PVDF chains resulting in the reduction of crystallinity (12.27%) which is lesser than that of PVDF-1 wt% CNF films. For 9 wt% CNF-loaded PVDF films, the crystallinity increases to 23.90% higher than that of PVDF-7 wt% CNF. Since 9 wt% CNF loading in PVDF corresponds to saturation in network formation and PVP would have coated the maximum number of CNF particles and there will be few CNF particles which might not have been coated completely by PVP as explained in the FTIR section to understand the variation in electroactive gamma phase content in the nanocomposites. The CNF particles would have resulted in agglomeration leading to enhanced crystallinity at that loading. The evidence for PVP coated CNF particles is reflected from the crystallization temperature (T_c) as T_c for all composites is lesser than that of neat PVDF with and without PVP. Since PVP is coated onto CNF particles which screens the interaction between PVDF and CNF, the crystallization is mainly due to solvent evaporation and the nucleating effect of CNF is not observed except for 9 wt% CNF loading in PVDF for which T_c is 140.3 °C. This value is slightly higher than that of neat PVDF.

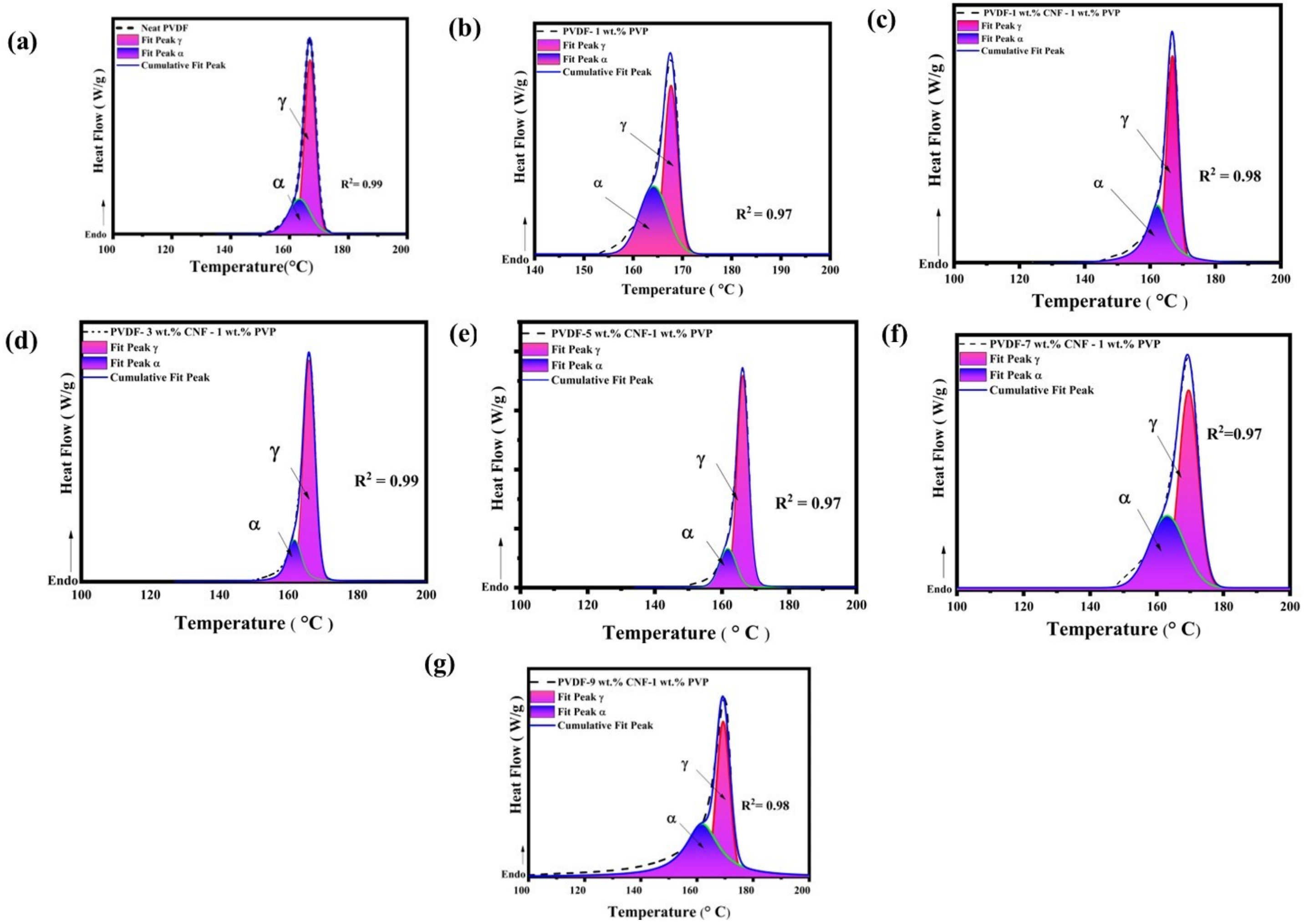

Fig. S7 (a)-(g) Deconvoluted DSC melting curves of PVDF-CNF-PVP nanocomposites.

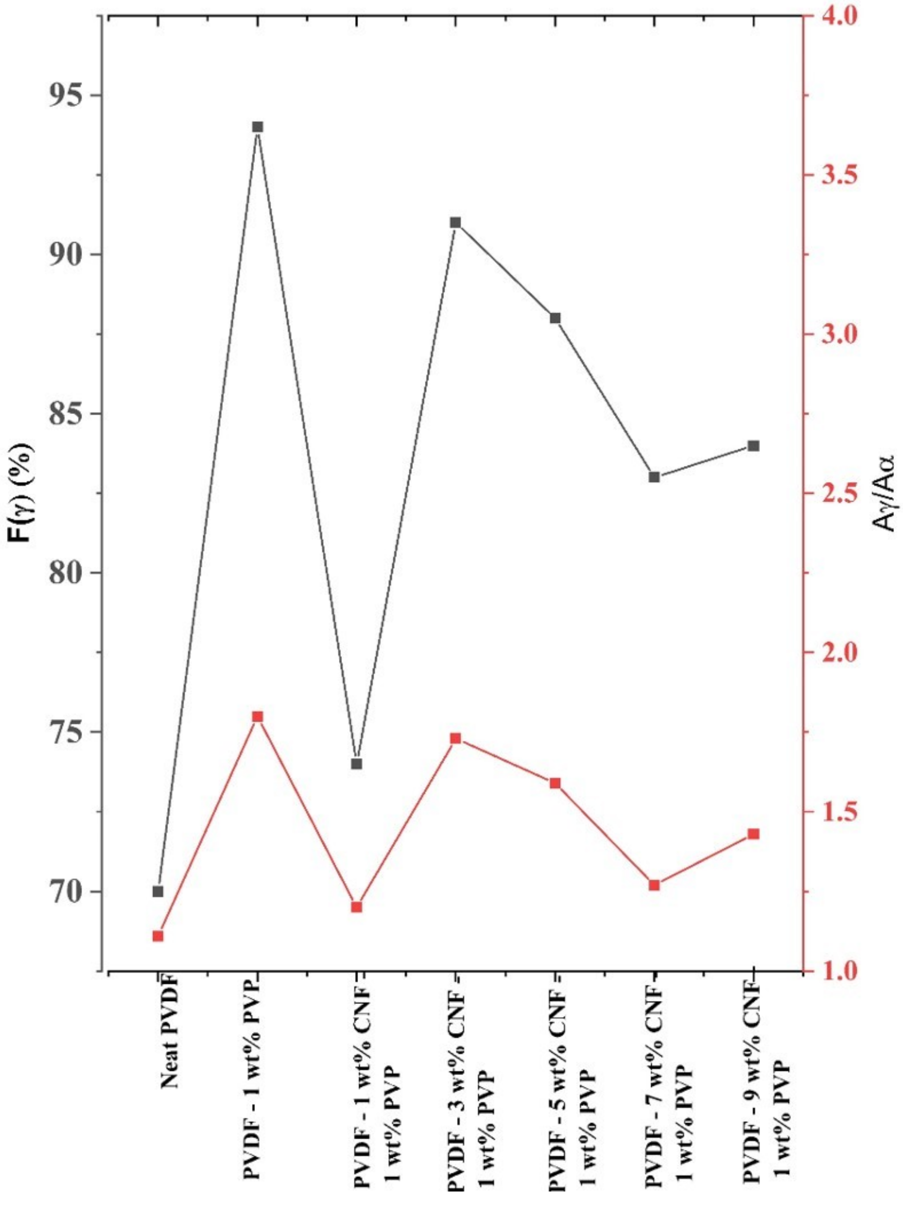
F(γ) (%)
95
90
85
80
75
70
Aγ/Aα
4.0
3.5
3.0
2.5
2.0
1.5
1.0
Neat PVDF
PVDF - 1 wt% PVP
PVDF - 1 wt% CNF 1 wt% PVP
PVDF - 3 wt% CNF 1 wt% PVP
PVDF - 5 wt% CNF 1 wt% PVP
PVDF - 7 wt% CNF 1 wt% PVP
PVDF - 9 wt% CNF 1 wt% PVP

Fig. S8 Comparison of gamma phase content and ratio of area under gamma phase melting curve to alpha phase melting curve obtained from deconvolution of melting curves of PVDF, PVDF-1 wt% PVP, and PVDF-x wt% CNF-1 wt% PVP (x=1,3,5,7,9).

The melting curves of neat PVDF, PVDF-1 wt% PVP, PVDF-x wt% CNF-1 wt% PVP (x=1,3,5,7,9) have been deconvoluted into two peaks, out of which one corresponds to alpha phase and the high temperature melting peak corresponds to gamma phase of PVDF as shown in Fig. S7a-g. The ratio of area under the gamma phase melting curve to the area under the alpha phase melting curve (A_γ/A_α) follows similar trend as that of electroactive gamma phase fraction in nanocomposites as obtained through FTIR analysis. The comparision between the above mentioned parameters is depicted in Fig. S8.

Table S3 Degree of crystallinity (X_c), crystallization temperature (T_c) and ratio of area under gamma crystal melting curve to the alpha crystal melting curve of PVDF-CNF nanocomposites.

Sample	**Degree of Crystallinity (X_c) (%)**	**Crystallization Temperature (T_c) (° C)**	**A_γ/A_α**
Neat PVDF	43.64	140.1	1.11
PVDF-1 wt% PVP	40.12	139. 2	1.80
PVDF-1 wt% CNF-1 wt% PVP	15.70	136.72	1.20
PVDF-3 wt% CNF-1 wt% PVP	30.14	137.12	1.73
PVDF-5 wt% CNF-1 wt% PVP	25.58	137.57	1.59
PVDF-7 wt% CNF-1 wt% PVP	12.27	137.72	1.27
PVDF-9 wt% CNF-1 wt% PVP	23.90	140.31	1.43

In short, the following conclusions can be arrived at from the DSC analysis of PVDF-CNF-PVP nanocomposites.

(1) The percentage of crystallinity decreases when CNF is incorporated in PVDF matrix with PVP in comparison to neat PVDF with PVP.

(2) The PVP chains coat onto CNF particles and hence the interaction between CNF and PVDF is screened.

(3) Coexistence of electroactive gamma and non-polar alpha phases of PVDF in PVDF-CNF nanocomposites.

The above results are consistent with electroactive phase analysis carried out through FTIR and XRD analyses.

S2.5. Quantification of the electroactive phase in PVDF-CNF-Fe_3O_4 hybrid nanocomposites

The quantification of electroactive gamma phase content of PVDF in hybrid nanocomposites has been carried out in a similar way to that of PVDF-CNF nanocomposites as described in section S2.3. The gamma fraction values are given in Table S4 below. There exists a slight increase in the gamma phase content with Fe_3O_4 incorporation in PVDF-9 wt% CNF nanocomposite. It should be noted that more than 84% gamma phase content remains in the hybrid nanocomposites. The variation of electroactive phase content can be understood in a similar manner to that of PVDF-CNF nanocomposites with PVP. Since magnetite nanoparticles occupy inter CNF spaces, effectively less PVP molecules are required to coil around as more ordered structure is formed. Hence, the interaction between PVP molecules present in the PVDF matrix with PVDF chains can improve electroactive gamma phase content. In short, in hybrid nanocomposites, more than 84% of electroactive phase content is present. The DSC analysis shows that T_c is not increased for hybrid nanocomposites in comparison to PVDF-9 wt% CNF with PVP. Thus, the nucleating effect of magnetite cannot exist and the enhancement in electroactive gamma phase can be explained in similar lines to that of binary nanocomposites. The result underscores the potential of hybrid nanocomposites to be used as piezoelectric nanogenerator and EMI shield which will be flexible and mechanically robust.

Table S4 Quantification of electroactive gamma phase in PVDF-9 wt% CNF-Fe_3O_4 hybrid nanocomposites with 1 wt% PVP.

Sample	**Gamma phase fraction (%)**
PVDF-9 wt% CN-1 wt % PVP	84.3 ± 0.2
PVDF-9 wt% CNF-1 wt% Fe_3O_4-1 wt % PVP	85.3 ± 0.1
PVDF-9 wt% CNF-3 wt% Fe_3O_4-1 wt % PVP	86.5 ± 0.1

S2.6. DSC analysis of PVDF-CNF-Fe_3O_4 hybrid nanocomposites

In order to ascertain the coexistence of electroactive gamma and non-polar alpha phases in hybrid nanocomposites, DSC crystallisation and melting curves of PVDF-9 wt% CNF-x wt% Fe_3O_4 (x=0,1,3) nanocomposites are presented in Fig. S9a and b.

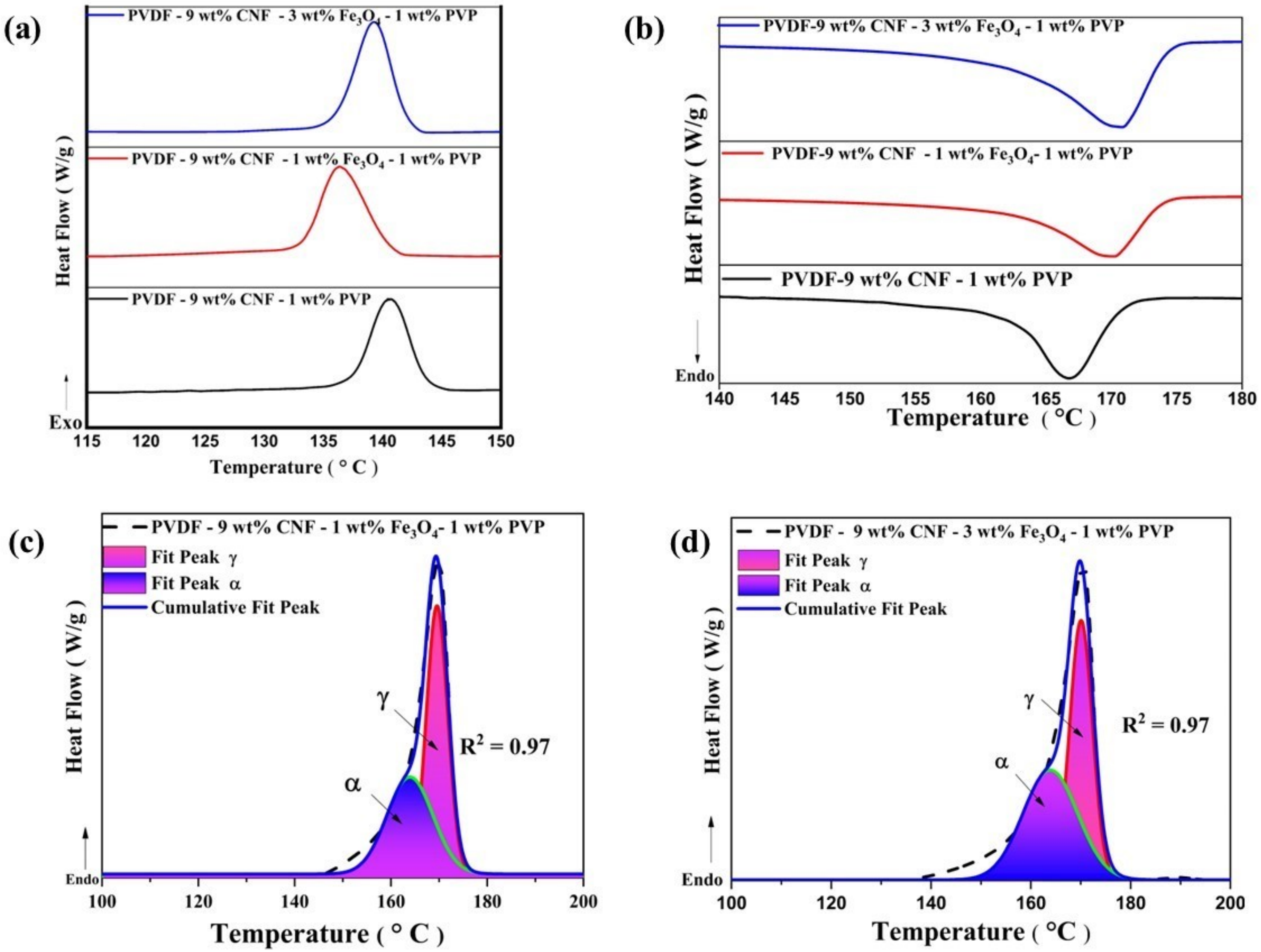

Fig. S9 DSC (a) crystallization, (b) melting curves of PVDF-CNF-Fe_3O_4 nanocomposites, deconvoluted melting curves of (c) PVD-9 wt% CNF-1 wt% Fe_3O_4 -1 wt% PVP, and (d) PVDF-9 wt% CNF-3 wt% Fe_3O_4 -1 wt% PVP.

The melting curves in the DSC corresponding to hybrid nanocomposites are deconvoluted using the Gaussian function and it can be seen that in hybrid nanocomposites two melting peaks one at ~162 °C corresponding to the alpha phase and the other at ~ 170 °C corresponding to the gamma phase of PVDF could be witnessed. Hence, the coexistence of both alpha and gamma phases can be confirmed which support XRD and FTIR results. The deconvoluted melting curves are shown in the Fig. S9c-d. In all the DSC plots, it is evident that the area under the gamma phase melting curve is higher than that of alpha phase melting curve which confirms the results obtained through XRD and FTIR analyses. Thus, incorporation of magnetite nanoparticles does not affect the phases, however the phase contents are different in comparison to PVDF-CNF nanocomposites with 1 wt% PVP. The gamma phase content in PVDF based hybrid nanocomposites is listed in Table S4.

The crystallization temperature (T_c) , degree of crystallinity (X_c) and ratio of area under gamma phase melting curve to alpha phase meting curve from the deconvoluted melting curves of hybrid nanocomposites are presented in Table S5. It can be seen from Table S5 that the crystallization temperature of hybrid nanocomposites decreases with the inclusion of magnetite nanoparticles in PVDF-CNF nanocomposites suggesting the fact that nanoparticle obstructs crystallization of PVDF chains. With 1 wt% Fe_3O_4 loading in hybrid nanocomposites, the T_c decreases by slightly above 3 °C in comparison to PVDF-9 wt% CNF with 1 wt% PVP. The crystallinity of the hybrid nanocomposite is decreased to 9.88 % from 23.90 % for PVDF-9 wt% CNF nanocomposites with PVP. This is attributed to the occupation of magnetite nanoparticles between PVDF chains impeding the crystallization process. It should be mentioned that electroactive phase content refers to the percentage of different phases within the crystallized region in the nanocomposites. With 3 wt% Fe_3O_4 incorporation in PVDF-9 wt% CNF composite, T_c is slightly increased in comparison to 1 wt% Fe_3O_4 loaded hybrid nanocomposites, suggesting the fact that magnetite particles could have been agglomerated locally. However, the electrical conductivity is enhanced as the occupation of these nanoparticles are in between CNFs so the charge transport becomes easier. The X_c is decreased further as these PVP coated magnetite nanoparticles can be present between PVDF chains and impeding the crystallization further. Thus, the variation of crystallinity in PVDF-CNF-Fe_3O_4 hybrid nanocomposites can be understood.

Table S5 Degree of crystallinity (X_c), crystallization temperature (T_c) and ratio of area under gamma phase to alpha phase melting curves obtained from the deconvoluted melting curves of hybrid nanocomposites PVDF-CNF-Fe_3O_4 nanocomposites.

Sample	**Degree of Crystallinity (X_c) (%)**	**Crystallization Temperature (T_c) (°C)**	**A_γ/A_α**
PVDF-9 wt% CNF-1 wt% PVP	23.90	140.3	1.43
PVDF-9 wt% CNF-1 wt% PVP-1 wt% Fe_3O_4	9.88	136.9	1.45
PVDF-9 wt% CNF-1 wt% PVP-3 wt% Fe_3O_4	9.47	139.8	1.49

References

1 Y. Huang, Y. Zheng, W. Song, Y. Ma, J. Wu and L. Fan, *Compos Part A Appl Sci Manuf*, 2011, **42**, 1398–1405.

2 X. Lu, M. Niu, R. Qiao and M. Gao, *J Phys Chem B*, 2008, **112**, 14390–14394.

3 Y. Zhu, H. Wang, H. Li and J. Zhu, *Journal of Wuhan University of Technology-Mater. Sci. Ed.*, 2016, **31**, 1219–1225.

4 D. Sebastián, I. Suelves, R. Moliner and M. J. Lázaro, *Carbon N Y*, 2010, **48**, 4421–4431.

5 Y. Zhao, J. Hou, Z. Bai, Y. Yang, X. Guo, H. Cheng, Z. Zhao, X. Zhang, J. Chen and C. Shen, *Compos Part A Appl Sci Manuf*, 2020, **139**, 106095.

6 M. Samet, V. Levchenko, G. Boiteux, G. Seytre, A. Kallel and A. Serghei, *J Chem Phys*, 2015, **142**, 194703.

7 Z. He, X. Yu, J. Yang, N. Zhang, T. Huang, Y. Wang and Z. Zhou, *Compos Part A Appl Sci Manuf*, 2018, **104**, 89–100.

8 L. M. Saleh Medina and R. M. Negri, *The Journal of Physical Chemistry C*, 2017, **121**, 27683–27692.

9 A. Rahal, S. M. Borchani, K. Guidara and M. Megdiche, *R Soc Open Sci*, 2018, **5**, 171472.

10 X. Cai, T. Lei, D. Sun and L. Lin, *RSC Adv*, 2017, **7**, 15382–15389.

11 Z. Guo, X. Xu, Y. Xiang, S. Lu and S. P. Jiang, *J Mater Chem A Mater*, 2015, **3**, 148–155.

12 J. Ayyappan, N. H. Menon, A. Sabu and B. T. S. Ramanujam, *Polym Adv Technol*, 2022, **33**, 3997–4011.

13 J. Liu, X. Lu and C. Wu, *Membranes (Basel)*, 2013, **3**, 389–405.

List of Figures

Fig. S1 Digital images of solution blended (a) PVDF-3 wt% CNF, (b) PVDF-3 wt% CNF-1 wt% PVP, (c) PVDF-3 wt% Fe_3O_4, (d) PVDF-3 wt% Fe_3O_4-1 wt% PVP, (e) PVDF-3 wt% CNF-3 wt% Fe_3O_4, and (f) PVDF-3 wt% CNF-3 wt% Fe_3O_4 -1 wt% PVP.

Fig. S2 Dispersion of (a) CNF, (b) magnetite nanoparticles in DMAc solvent without PVP, (c) CNF dispersion with PVP after 30 mins probe sonication, (d) magnetite dispersion with PVP after 30 mins probe sonication, (e) CNF dispersion with PVP after 15 hours probe sonication, and (f) magnetite dispersion with PVP after 15 hours probe sonication.

Fig. S3 (a) AC Conductivity, and (b) real part of relative permittivity of PVDF-CNF nanocomposites.

Fig. S4 (a)-(d) Impedance plots of solution blended PVDF-x wt% CNF (x=3,5,7,9) nanocomposite with 1 wt% PVP, and (e) schematic of the proposed equivalent circuit.

Fig. S5 Model depicting the interaction between PVDF, CNF and PVP.

Fig. S6 (a) Crystallization, and (b) melting curves of PVDF-CNF solution blended nanocomposites with PVP.

Fig. S7 (a)-(g) Deconvoluted DSC melting curves of PVDF-CNF-PVP nanocomposites.

Fig. S8 Comparison of gamma phase content and ratio of area under gamma phase melting curve to alpha phase melting curve obtained from deconvolution of melting curves of PVDF, PVDF-1 wt% PVP and PVDF-x wt% CNF-1 wt% PVP (x=1,3,5,7,9).

Fig. S9 DSC (a) crystallization, (b) melting curves of PVDF-CNF-Fe_3O_4 nanocomposites, deconvoluted melting curves of (c) PVD-9 wt% CNF-1 wt% Fe_3O_4 -1 wt% PVP, and (d) PVDF-9 wt% CNF-3 wt% Fe_3O_4 -1 wt% PVP.

List of Tables

Table S1 Parameters extracted from impedance plots of PVDF-x wt% CNF (x=3,5,7,9) with 1 wt% PVP after fitting to parallel model.

Table S2 Quantification of electroactive gamma phase content in solution blended neat PVDF, PVDF-x wt% CNF-1 wt% PVP (x=0,1,3,5,7,9) films.

Table S3 Degree of crystallinity (X_c), crystallization temperature (T_c) and ratio of area under gamma crystal melting curve to the alpha crystal melting curve of PVDF-CNF nanocomposites.

Table S4 Quantification of electroactive gamma phase in PVDF-9 wt% CNF-Fe_3O_4 hybrid nanocomposites with 1 wt% PVP.

Table S5 Degree of crystallinity (X_c), crystallization temperature (T_c) and ratio of area under gamma phase to alpha phase melting curves obtained from the deconvoluted melting curves of hybrid nanocomposites PVDF-CNF-Fe_3O_4 nanocomposites